Available online at www.eccomasproceedia.org
Eccomas Proceedia SMART (2023) 607-618

ECCOMAS
Proceedia

X ECCOMAS Thematic Conference on Smart Structures and Materials
SMART 2023
D.A. Saravanos, A. Benjeddou, N. Chrysochoidis and T. Theodosiou (Eds)

# EFFICIENT LAYERWISE THEORY-BASED TIME-DOMAIN SPECTRAL ELEMENT FOR COMPOSITE STRIPS WITH PIEZO PATCHES APPLYING HYBRID POINT-LEAST SQUARES CONTINUITY AT PATCH FRONTS

**MAYANK JAIN* AND SANTOSH KAPURIA†**

(*†)Indian Institute of Technology Delhi, Hauz Khas 110016, Delhi, India
*e-mail: jainmayank135@gmail.com, †e-mail: kapuria@am.iitd.ac.in

**Abstract.** This article presents the efficient electromechanically coupled layerwise zigzag theory (ZIGT)-based time-domain spectral element (TDSE) for analyzing the composite beam/panel (strip) with piezo patches bonded on its top/bottom surface. The ZIGT assumes in-plane displacement $u$ to follow global third-order with linear layerwise variation and piecewise quadratic electric potential variation across the thickness. Transverse displacement $w$ accommodates electric field-induced normal deformation. Since $u$-variation differs for the host laminate and the laminate with the patch transducer, we maintain continuity at the intersection of both laminates using the newly developed hybrid point-least squares method. We perform static and free vibration analyses of composite strips with surface-bonded patch piezo actuators and sensors under mechanical and electrical potential loadings. We develop a continuum-based FE solution in ABAQUS to assess the accuracy of the proposed model. It is found to be a highly accurate and computationally efficient tool for modelling such smart structures.

**Key words:** Time domain spectral element, Zigzag theory, Composite strip, Piezoelectric patch, Patch front, Hybrid continuity method

## 1 INTRODUCTION

Lightweight anisotropic fiber-reinforced composites replace isotropic metals in modern structures like aircraft, spaceships, cars, marine propellers, wind turbine blades, bridges, and medical equipment. However, due to their complex failure modes, such as delaminations, they need real-time structural health monitoring (SHM) for their overall performance and improved reliability [1]. The patches of piezoelectric ceramics, polymers, and macro fiber composites are commonly employed as sensors and actuators for such purposes [2]. Thus, modelling such piezoelectric patches is essential in accurately analyzing smart structures. However, much less attention has been paid to its accurate modelling.

The most popular choice for solving boundary value problems in complex geometries is the conventional FEM. It has been used for modelling laminated structures with piezoelectric


Peer-review under responsibility of the organizing committee of SMART 2023.
doi: 10.7712/150123.9815.444768

patches bonded on their top surfaces using the equivalent single layer (ESL) theories such as first-order shear deformable theory (FSDT) [3] and the refined third-order theory (TOT) [4]. Since for the higher order theories having non-linear displacement field variation, the host laminate and the laminates with bonded piezoelectric patches have different displacement fields due to differences in thickness and lay-up, we must satisfy the continuity across the intersection of the adjacent laminates (patch fronts). However, the model based on the TOT [4] does not employ any continuity criteria for satisfying the continuity of displacement field variables at the patch fronts.

On the other hand, ESL theories are computationally efficient but less accurate than layerwise theories (LWTs). It is due to the layerwise description of displacement field variation across the laminate thickness in the LWTs. However, the LWTs yield high computational efforts due to the large number of degrees of freedom (DOFs) for modelling purposes. Electromechanically coupled efficient layerwise theories (ELTs) or zigzag theories (ZIGTs) have been developed to overcome this issue. No study was available using such theories with non-linear displacement field variation for the piezo patch modelling based on the continuity criteria until Kapuria and Ahmed [5] developed the ZIGT-based FE model to analyze laminated plates with bonded piezoelectric patches. This model employs a recently developed hybrid point-least squares continuity (HPLSC) method to satisfy the continuity of the non-linear displacement field across the patch fronts.

Since conventional FE exhibits significant numerical dispersion and dissipation errors while performing high-frequency wave propagation analysis [6], a special-purpose FE, called the time-domain spectral element (TDSE) has been developed for overcoming such issues and simultaneously retaining all of the advantages of conventional FE. All of the studies have TDSEs based on $C^0$-continuous interpolation function for the displacement variables [7] until the authors have developed the $C^1$-continuous TDSEs based on the Euler Bernoulli theory [8], the TOT [9, 10], and the ZIGT [11] for wave propagation analysis of laminated structures. To the best of the authors' knowledge, no TDSEs have been developed for modelling laminated structures with piezoelectric patches on their top and bottom surfaces.

In this article, we develop a TDSE based on the ZIGT for dynamic analysis of laminated strips with surface-bonded piezoelectric patches using the HPLS continuity method for satisfying the continuity at the patch fronts. The formulation employs the efficient layerwise ZIGT, which has a high accuracy of the LWTs and computational efficiency of the ESL theories. The spectral element can have $n$-nodes having four mechanical DOFs (deflection $w_0$, slope $\frac{\mathrm{d}w_0}{\mathrm{d}x}$, axial displacement $u_0$, and rotation variable $\psi_0$) and a electric DOF (electric potential $\phi_c^l$) per node. For the continuity requirement of the ZIGT, we employ $C^1$-continuous spectral interpolations for $w_0$ and $\frac{\mathrm{d}w_0}{\mathrm{d}x}$, and $C^0$-continuous spectral shape functions for $u_0$, $\psi_0$, and $\phi_c^l$. A comprehensive numerical study has been performed to evaluate the performance of the developed TDSE for the analyses of the laminated structures with bonded piezo-patch in comparison with the continuum-based FE solution.

## 2 ZIGT-BASED SPECTRAL ELEMENT FORMULATION

Consider a laminated composite strip having any lay-up and piezoelectric patches bonded at its top and bottom surfaces. The total thickness $h$ and number of layers $L$ of such hybrid beams can vary segment-wise. The constitutive relations for such strips can be derived using plane stress and strain assumptions, which relate the normal stress $\sigma_x$, transverse shear stress $\tau_{zx}$, and electric displacements $D_i$ to the corresponding strains ($\varepsilon_x$ and $\gamma_{zx}$) and electric fields $E_i$ as

$$\begin{Bmatrix} \sigma_x \\ \tau_{zx} \\ D_x \\ D_z \end{Bmatrix} = \begin{bmatrix} \hat{Q}_{11} & 0 & \hat{e}_{11} & \hat{e}_{31} \\ 0 & \hat{Q}_{55} & \hat{e}_{15} & \hat{e}_{35} \\ \hat{e}_{11} & \hat{e}_{15} & -\hat{\eta}_{11} & -\hat{\eta}_{13} \\ \hat{e}_{31} & \hat{e}_{35} & -\hat{\eta}_{13} & -\hat{\eta}_{33} \end{bmatrix} \begin{Bmatrix} \varepsilon_x \\ \gamma_{zx} \\ -E_x \\ -E_z \end{Bmatrix} \tag{1}$$

where $\hat{Q}_{11}$ and $\hat{Q}_{55}$ are reduced stiffness coefficients, and $\hat{e}_{ij}$ and $\hat{\eta}_{ij}$ depend on the piezoelectric material parameters. The potential field $\phi$ is assumed as piecewise quadratic between $n_\phi$ points $z = z_\phi^j,\ j = 1, 2, \ldots, n_\phi$, across the thickness of the laminate as

$$\phi(x, z, t) = \Psi_\phi^j(z)\phi^j(x, t) + \Psi_c^l(z)\phi_c^l(x, t) \tag{2}$$

where $\Psi_\phi^j$ and $\Psi_c^l$ are the piecewise linear and quadratic functions of $z$, and $\phi_c^l(x, t)$ is the quadratic component of electric potential at $z = (z_\phi^l + z_\phi^{l+1})/2$. For the approximation of the deflection $w$, we integrate the constitutive equation for transverse normal strain $\varepsilon_z$ and obtain the deflection as

$$w(x, z, t) = w_0(x, t) - \bar{\Psi}_\phi^j(z)\phi^j(t) - \bar{\Psi}_c^l(z)\phi_c^l(t), \tag{3}$$

where

$$\bar{\Psi}_\phi^j(z) = \int_0^z d_{33}^k \Psi_{\phi,z}^j(z)\, dz, \qquad \bar{\Psi}_c^l(z) = \int_0^z d_{33}^k \Psi_c^l(z)\, dz. \tag{4}$$

where $w_0$ is the mid-plane deflection and $d_{33}^k$ is the piezoelectric coefficient of the $k^{\text{th}}$-layer. According to the ZIGT, the in-plane displacement $u$ follows a global third-order variation with a layerwise linear variation across the laminate thickness. The displacement field is assumed to be independent of $y$-direction for both plane stress and strain assumptions. Thus, the in-plane displacement $u$ is approximated as

$$u(x, z, t) = u_k(x, t) - z w_{0,x} + z\psi_k(x, t) + z^2\xi(x, t) + z^3\eta(x, t), \tag{5}$$

where $\square_{,x}$ denotes $\frac{\partial \square}{\partial x}$, $u_k$ and $\psi_k$ denote the axial and rotation displacements for layer $k$, and $\xi$ and $\eta$ are the quadratic and cubic components. In the ZIGT, the computational efficiency is achieved by eliminating $2L$ variables from the total $2L + 3$ variables by imposing $2(L - 1)$ continuity conditions of transverse shear stress $\tau_{zx}$ and in-plane displacement $u$ at each layer interface, and two conditions of shear traction-free surfaces at its top and bottom. After elimination, the displacement field can be expressed in terms of only three primary variables as

$$u(x, z, t) = u_0(x, t) - z w_{0_{,x}}(x, t) + R^k(z)\psi_0(x, t) \tag{6}$$

where $u_0$ and $\psi_0$ denote the axial and rotation displacements at the mid-plane ($z = 0$), and $R_k(z)$ is the layerwise cubic function of $z$ for any layer $k$. Hamilton's principle for the hybrid strips subjected to normal transverse loading $q_z(x)$ per unit area reduces to

$$\int_{x^e} [\langle \rho^k(x)\ddot{u}\delta u + \rho^k(x)\ddot{w}\delta w + \sigma_x\delta\varepsilon_x + \tau_{zx}\delta\gamma_{zx} - D_x\delta E_x - D_z\delta E_z\rangle + bq_z(x)\delta w + bD_z\delta\phi]\,\mathrm{d}x b(x)\langle\bar{\sigma}_x\delta u + \bar{\tau}_{zx}\delta w + D_x\delta\phi\rangle\big|_x = 0, \qquad \forall\,\delta u_0, \delta w \tag{7}$$

where the notation $\langle \ldots \rangle = \sum_{k=1}^{L}\int_{z_{k-1}^+}^{z_k^-}(\ldots)b\,dz$, $\rho_k$ is the material mass density of the layer $k$, and $b$ is the beam width (=1 for infinite panels). In the current spectral element formulation, $u_0$ and $\psi_0$ are interpolated using the $C^0$-continuous spectral interpolations $\mathbf{N}$, whereas $C^1$-continuous spectral shape functions $\bar{\mathbf{N}}$ interpolates $w_0$ based on the continuity criteria of the ZIGT. The details of these functions can be found in [8]. Thus, the field variables can be interpolated in an $n$-node spectral element as

$$u_0 = \mathbf{N}\boldsymbol{u_0^e}, \qquad \psi_0 = \mathbf{N}\boldsymbol{\psi_0^e}, \qquad w_0 = \bar{\mathbf{N}}\boldsymbol{w_0^e}, \qquad \phi_c^l = \mathbf{N}\boldsymbol{\phi_c^{le}} \tag{8}$$

with

$$\begin{aligned} \boldsymbol{u_0^e} &= \begin{bmatrix} u_{0_1} & u_{0_2} & \ldots & u_{0_n} \end{bmatrix}^{\mathrm{T}}, \quad \boldsymbol{\psi_0^e} = \begin{bmatrix} \psi_{0_1} & \psi_{0_2} & \ldots & \psi_{0_n} \end{bmatrix}^{\mathrm{T}} \\ \boldsymbol{w_0^e} &= \begin{bmatrix} w_{0_1} & \theta_1 & w_{0_2} & \theta_2 & \ldots & w_{0_n} & \theta_n \end{bmatrix}^{\mathrm{T}}, \boldsymbol{\phi_c^{le}} = \begin{bmatrix} \phi_c^{l^1} & \phi_c^{l^2} & \ldots & \phi_c^{l^n} \end{bmatrix}^{\mathrm{T}} \end{aligned} \tag{9}$$

Defining the element displacement vector $\mathbf{U}^{e^{\mathrm{T}}} = [\boldsymbol{u_0^{e^{\mathbf{T}}}} \quad \boldsymbol{w_0^{e^{\mathbf{T}}}} \quad \boldsymbol{\psi_0^{e^{\mathbf{T}}}} \quad \boldsymbol{\phi_c^{l^{e^{\mathbf{T}}}}} \quad \phi^j]$, with $\phi_j$ constant over an element. Using the variational equation (7) and Eq. (8), we have the element mass matrix $\bar{\mathbf{M}}^e$, stiffness matrix $\bar{\mathbf{K}}^e$ and load vector $\bar{\mathbf{P}}^e$ as

$$\bar{\mathbf{M}}^e = \frac{l^e}{2}\int_{-1}^{1}\hat{\mathbf{N}}^{\mathrm{T}}\tilde{\mathbf{I}}\hat{\mathbf{N}}\,\mathrm{d}\xi, \quad \bar{\mathbf{K}}^e = \frac{l^e}{2}\int_{-1}^{1}\hat{\mathbf{B}}^{\mathrm{T}}\bar{\mathbf{D}}\hat{\mathbf{B}}\,\mathrm{d}\xi, \quad \bar{\mathbf{P}}^e = \frac{l^e}{2}\int_{-1}^{1}\hat{\mathbf{N}}^{\mathrm{T}}\boldsymbol{f_u}\,\mathrm{d}\xi. \tag{10}$$

where $\bar{\mathbf{D}}$ and $\tilde{\mathbf{I}}$ denote the stiffness coefficient matrix and inertia matrix, respectively, which depends on the material properties and lay-up of the beam. Matrix $\hat{\mathbf{N}}$ and $\hat{\mathbf{B}}$ are given by

$$\hat{\mathbf{N}} = \begin{bmatrix} \mathbf{N} & \mathbf{0} & \mathbf{0} & \mathbf{0} & \mathbf{0} \\ \mathbf{0} & -\frac{2}{l^e}\frac{\mathrm{d}\bar{\mathbf{N}}}{\mathrm{d}\xi} & \mathbf{0} & \mathbf{0} & \mathbf{0} \\ \mathbf{0} & \mathbf{0} & \mathbf{N} & \mathbf{0} & \mathbf{0} \\ \mathbf{0} & \bar{\mathbf{N}} & \mathbf{0} & \mathbf{0} & \mathbf{0} \\ \mathbf{0} & \mathbf{0} & \mathbf{0} & \mathbf{0} & \mathbf{I}_{n_\phi\times n_\phi} \end{bmatrix}, \qquad \hat{\mathbf{B}} = \begin{bmatrix} \frac{2}{l^e}\frac{\mathrm{d}\mathbf{N}}{\mathrm{d}\xi} & \mathbf{0} & \mathbf{0} & \mathbf{0} & \mathbf{0} \\ \mathbf{0} & -\frac{4}{l^{e2}}\frac{\mathrm{d}^2\bar{\mathbf{N}}}{\mathrm{d}\xi^2} & \mathbf{0} & \mathbf{0} & \mathbf{0} \\ \mathbf{0} & \mathbf{0} & \frac{2}{l^e}\frac{\mathrm{d}\mathbf{N}}{\mathrm{d}\xi} & \mathbf{0} & \mathbf{0} \\ \mathbf{0} & \mathbf{0} & \mathbf{N} & \mathbf{0} & \mathbf{0} \\ \mathbf{0} & \mathbf{0} & \mathbf{0} & -\frac{2}{l^e}\frac{\mathrm{d}\mathbf{N}}{\mathrm{d}\xi} & \mathbf{0} \\ \mathbf{0} & \mathbf{0} & \mathbf{0} & \frac{2}{l^e}\frac{\mathrm{d}\mathbf{N}}{\mathrm{d}\xi} & \mathbf{0} \\ \mathbf{0} & \mathbf{0} & \mathbf{0} & \mathbf{N} & \mathbf{0} \\ \mathbf{0} & \mathbf{0} & \mathbf{0} & \mathbf{0} & \mathbf{I}_{n_\phi\times n_\phi} \end{bmatrix}. \tag{11}$$

### 2.1 Continuity at the patch front

Since the displacement field is nonlinear and depends on the thickness of the laminate, it is different for the primary laminate (P) in the elastic substrate and the secondary laminate (S) in the hybrid part. For maintaining continuity at the intersection of these laminates (patch fronts), we use the hybrid point least squares continuity (HPLSC) method. In this method, the in-plane displacements of both laminates are made to be exactly equal at the mid-plane of the primary laminate, whereas the rotation variables ($w_{0,x}$ and $\psi_0$) are determined by minimizing the norm $F$ of the deviation between $u^S$ and $u^P$, i.e., $F = \sum_{k=b+1}^{b+p} \int_{z_{k-1}}^{z_k} (u^P - u^S)^2 \, dz$ over the common interface, which is given as

$$u^S(x, y, -z_c, t) = u^P(x, y, 0, t), \qquad \frac{\partial F}{\partial w^P_{0,x}} = 0, \qquad \frac{\partial F}{\partial \psi^P_0} = 0 \tag{12}$$

Equation (12) constitutes the continuity conditions for the HPLSC method, which yields the following relations:

$$\begin{aligned} u^S_0 - u^P_0 + z_c w^S_{0,x} + R^k_S(-z_c)\psi^S_0 &= 0 \\ a_1 w^S_{0,x} - a_1 w^P_{0,x} + a_2 \psi^P_0 - a_3 \psi^S_0 &= 0 \\ b_1 u^P_0 - b_1 u^S_0 - b_2 w^P_{0,x} + b_3 w^S_{0,x} + b_4 \psi^P_0 - b_5 \psi^S_0 &= 0 \end{aligned} \tag{13}$$

where the coefficients $a_i$ and $b_i$ depend on the lay-up and material properties of the laminate. From the above relations, we can obtain the transformation matrix $\mathbf{T}_i$ for any node $i$ in an $n$-node element as

$$\begin{bmatrix} u^S_0 & w^S_0 & w^S_{0,x} & \psi^S_0 \end{bmatrix}^{\mathrm{T}} = \mathbf{T}_i \begin{bmatrix} u^P_0 & w^P_0 & w^P_{0,x} & \psi^P_0 \end{bmatrix}^{\mathrm{T}}, \tag{14}$$

Accordingly, the stiffness and mass matrices of the elements in the patched segment on the patch front are transformed as $\mathbf{M}^e = \mathbf{T}_e^{\mathrm{T}} \bar{\mathbf{M}}^e \mathbf{T}_e$, $\mathbf{K}^e = \mathbf{T}_e^{\mathrm{T}} \bar{\mathbf{K}}^e \mathbf{T}_e$, and $\mathbf{P}^e = \mathbf{T}_e^{\mathrm{T}} \bar{\mathbf{P}}^e$, with

$$\mathbf{T}_e = \begin{bmatrix} \mathbf{T}_1 & & & & \\ & \mathbf{I}_4 & & & \\ & & \dots & & \\ & & & \mathbf{I}_4 & \\ & & & & \mathbf{T}_n \end{bmatrix} \tag{15}$$

where $\mathbf{I}_4$ is the identity matrix of size $4 \times 4$. Finally, we develop the global equation of motion by summing up the contribution of total $n_e$ spectral finite element using the standard assembly procedure, given as

$$\mathbf{M}\ddot{\mathbf{U}} + \mathbf{C}\dot{\mathbf{U}} + \mathbf{K}\mathbf{U} = \mathbf{P}. \tag{16}$$

where $\mathbf{M}$ and $\mathbf{K}$ are the assembled mass and stiffness matrices, whereas $\mathbf{U}$ and $\mathbf{P}$ denote the global displacement and load vector, respectively. Using Rayleigh hypothesis, damping term $\mathbf{C}\dot{\mathbf{U}}$ has been incorporated in Eq. (16) to account for any viscous damping. The damping matrix $\mathbf{C} = \alpha_1 \mathbf{M} + \alpha_2 \mathbf{K}$, where $\alpha_1$ and $\alpha_2$ are the mass and stiffness damping coefficients, respectively.

## 3 NUMERICAL RESULTS AND DISCUSSIONS

In this section, we first validate the proposed formulation and developed computer program for static and stress analyses of multi-layered beams with piezoelectric patches bonded at their top surface under mechanical and electrical loadings. The piezo elasticity-based continuum FE solutions are employed to validate and assess the accuracy of the SE-based patch modelling, since such solutions do not make any prior assumptions on the variations of the displacement field across the laminate thickness. We next perform the free vibration analysis of such hybrid beams and compare the relative performances of the present method with and without satisfying the continuity of displacement field at patch fronts with respect to the continuum-based FE solutions.

### 3.1 Static and stress analysis

In this example, we consider a cantilever beam having a piezoelectric patch (PZT-5A) layer bonded on the top of the elastic substrate (shown in Fig. 1). The elastic substrate of length $a$, width $b = 10$ mm and total thickness $h$ is made of a four-layer graphite/epoxy (Gr/Ep) composite with a lay-up $[0°/90°]_S$ and equal thickness per layer. The piezoelectric patch is made of a PZT-5A layer with length $a_p = 0.4a$ and thickness $h_p = 0.1h$. The material properties of Gr/Ep and PZT-5A are shown in Table 1.

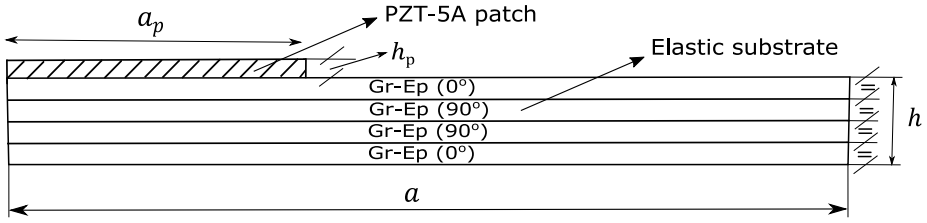


**Figure 1**: Geometry of laminated composite beam with piezoelectric patch

**Table 1**: Material properties

| | $Y_1$ | $Y_2$ | $Y_3$ | $G_{23}$ | $G_{13}$ | $G_{12}$ | $\nu_{12}$ | $\nu_{13}$ | $\nu_{23}$ | $\rho$ |
|---|---|---|---|---|---|---|---|---|---|---|
| Material | (GPa) | | | | | | | | | (kg/m$^3$) |
| Gr/Ep [12] | 181.0 | 10.3 | 10.3 | 2.87 | 7.17 | 7.17 | 0.28 | 0.28 | 0.33 | 1578 |
| PZT-5A [13] | 61.0 | 61.0 | 53.2 | 21.1 | 21.1 | 22.6 | 0.35 | 0.35 | 0.38 | 7600 |
| | $d_{31}$ | $d_{32}$ | $d_{33}$ | $d_{15}$ | $d_{24}$ | | $\eta_{11}$ | $\eta_{22}$ | $\eta_{33}$ | |
| | ($\times 10^{-12}$mV$^{-1}$) | | | | | | ($\times$ $10^{-9}$ F/m) | | | |
| PZT-5A [13] | -171 | -171 | -374 | 584 | 584 | | 15.3 | 15.3 | 15.0 | |

We consider two load cases with $\phi = 0$ at the interface between the elastic laminate and the PZT-5A layer, which are shown in Fig. 2 and are described as

**Load case 1 (mechanical loading):** uniform pressure $-p_0$ on the top of the elastic laminate over a length of $a/20$ from the free end with $\phi = 0$ on the top of PZT.

**Load case 2 (potential loading):** uniform applied potential $\phi = \phi_0$ on the top of PZT.

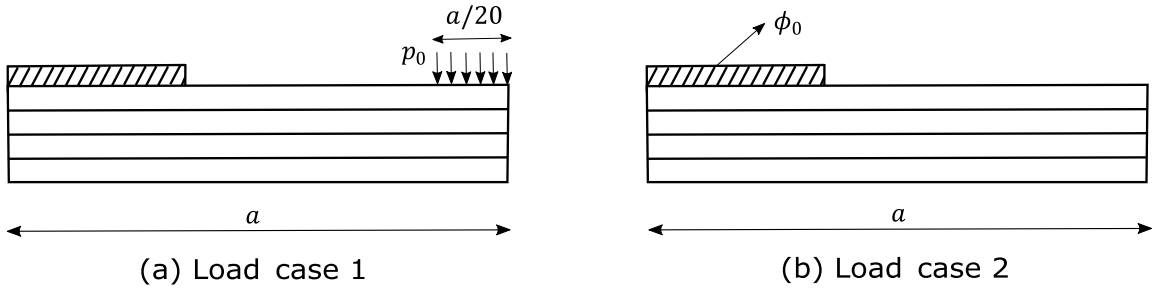


**Figure 2**: Different load cases considered for the static and stress analysis: (a) mechanical loading and (b) potential loading

The beam is divided into two separate segments for the elastic part and the hybrid part with PZT-patch. For the converged solutions, we employ 5 eight-node SEs (two for hybrid part and three for elastic part). The present results are validated and assessed with the continuum-based FE solution obtained by employing eight-node quadrilateral plane stress element (CPS8R) in commercial software ABAQUS, which is considered as the reference solution. In this 2D FE model, we employ a mesh of $100 \times 12$ (length $\times$ thickness) CPS8R elements in elastic substrate and $40 \times 2$ elements in PZT-patch layer. The transverse displacement $w$, axial stress $\sigma_x$, and the electric displacement $D_z$ for the two load cases are non-dimensionalised as

**Load case 1:** $\bar{w} = \dfrac{100 w Y_0}{h S^4 p_0}$, $\bar{\sigma}_x = \dfrac{\sigma_x}{S^2 p_0}$, $\bar{D}_z = \dfrac{10 D_z}{d_0 S^2 p_0}$.

**Load case 2:** $\hat{w} = \dfrac{10 w}{S^2 d_0 \phi_0}$, $\hat{\sigma}_x = \dfrac{\sigma_x h}{10 Y_0 d_0 \phi_0}$, $\hat{D}_z = \dfrac{D_z h}{100 Y_0 d_0^2 \phi_0}$.

where $S\ (= a/h)$ is span to thickness ratio, $Y_0 = 10.3$ GPa, and $d_0 = 374 \times 10^{-12}$ CN$^{-1}$.

We obtain the mid-plane deflection $w(l, 0)$ at the free end, the maximum axial stress $\sigma_x$ in the substrate and the piezoelectric layer, and the electric displacement $D_z$ at the top of the PZT at the center of piezo-patch ($x = 0.2l$), which are presented in Table 2 for both mechanical and potential loadings. We observe from the table that the present results are in excellent agreement with the continuum-based FE solution for beams with $S = 10$ and 20 under both load cases. Further, we plot the mid-plane deflection across the span of the beam with $S = 10$ for both load cases, shown in Fig. 3. Again, the present solution matches the reference solution very well for both cases of loadings. These results establishes the accuracy of the proposed ZIGT-based SE model using the HPLSC method of continuity at patch fronts.

Next, we obtain the maximum axial stress $\sigma_x$ in the elastic substrate and the piezoelectric layer along the span of the beam with $S = 10$ for both mechanical and potential loadings, represented in Fig. 4 and 5, respectively. The stresses apart from the edges are in excellent agreement with the continuum-based FE solution for the thick beam with $S = 10$. The localized stresses near the free edge of the PZT patch, which are secondary in nature do not, however, match well with the continuum solution. This deviation of local stresses in the proposed method may be due to the assumption of zero transverse normal stress $\sigma_z$ and that the layerwise variation of the in-plane displacement field to be linear only. Due to such reasons, most of the 1D and 2D

**Table 2**: Comparison of static response with continuum-based 2D FE solution for mechanical and potential loading

| | Non-dimensional | load-case 1 | | | Non-dimensional | load-case 2 | | |
|---|---|---|---|---|---|---|---|---|
| | entity | Present | 2D FE | % error | entity | Present | 2D FE | % error |
| $S=10$ | $\bar{w}(l,0)$ | -1.2821 | -1.2906 | -0.65 | $\hat{w}(l,0)$ | -3.1097 | -3.0353 | 2.45 |
| | $\bar{\sigma}_x(0.2l,0.6h)$ | 0.0895 | 0.0900 | -0.59 | $\hat{\sigma}_x(0.2l,0.5h^+)$ | -2.2816 | -2.2767 | 0.22 |
| | $\bar{\sigma}_x(0.2l,-0.5h)$ | -0.2486 | -0.2489 | -0.12 | $\hat{\sigma}_x(0.2l,0.5h^-)$ | 1.2688 | 1.2871 | -1.43 |
| | $\bar{D}_z(0.2l,0.6h)$ | -0.3802 | -0.3722 | 2.13 | $\hat{D}_z(0.2l,0.6h)$ | -1.5023 | -1.4657 | 2.49 |
| $S=20$ | $\bar{w}(l,0)$ | -1.1676 | -1.1694 | -0.16 | $\hat{w}(l,0)$ | -3.0777 | -3.0144 | 2.10 |
| | $\bar{\sigma}_x(0.2l,0.6h)$ | 0.0894 | 0.0898 | -0.38 | $\hat{\sigma}_x(0.2l,0.5h^+)$ | -2.2816 | -2.2825 | -0.04 |
| | $\bar{\sigma}_x(0.2l,-0.5h)$ | -0.2485 | -0.2485 | 0.01 | $\hat{\sigma}_x(0.2l,0.5h^-)$ | 1.2683 | 1.2685 | -0.02 |
| | $\bar{D}_z(0.2l,0.6h)$ | -0.3781 | -0.3714 | 1.81 | $\hat{D}_z(0.2l,0.6h)$ | -1.5024 | -1.4729 | 2.00 |

laminate theories cannot capture the local stresses properly. Note that, the maximum allowable limit for local stresses would be 2 to 3 times of that for the the primary stresses.

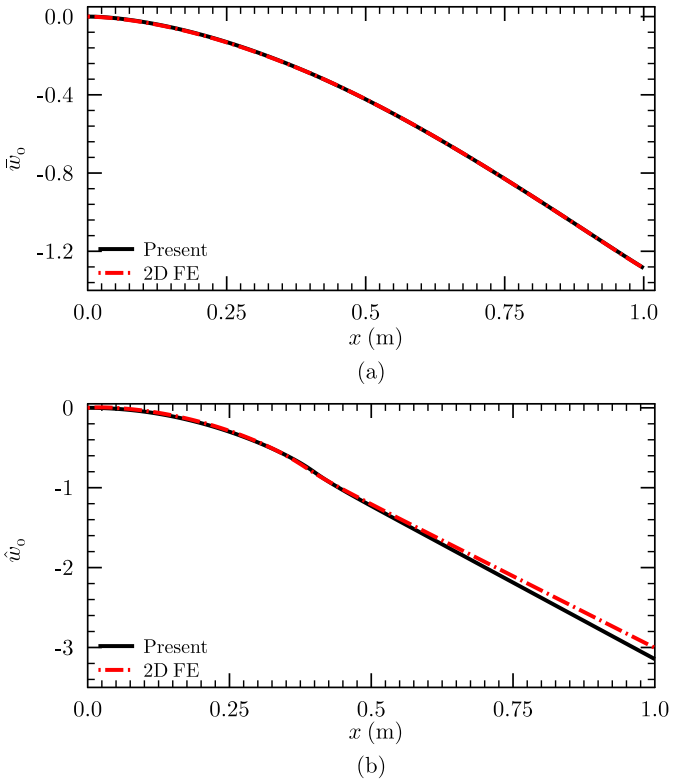


**Figure 3**: The mid-plane deflection across the length of the beam ($S=10$) under (a) load case 1 ($\bar{w}_0$) and (b) load case 2 ($\hat{w}_0$): Comparison with continuum-based FE solution.

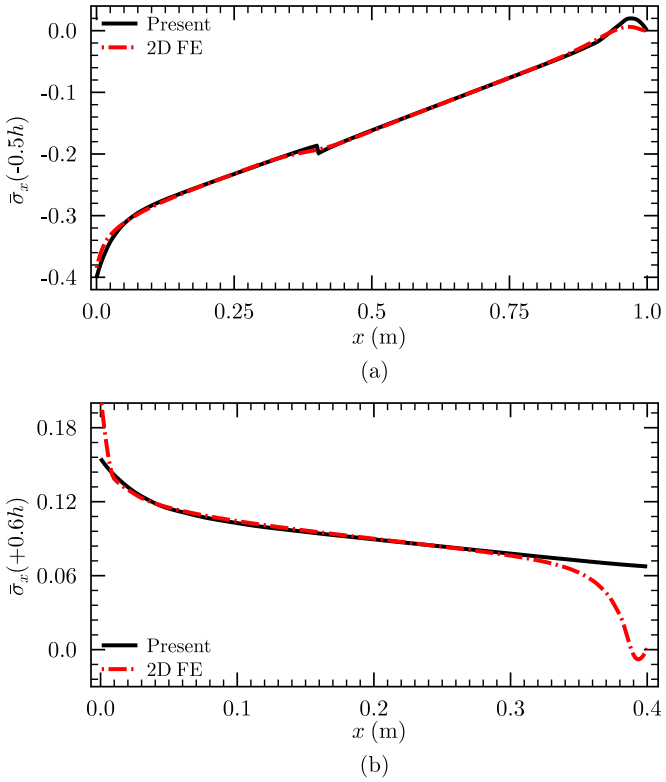


**Figure 4**: Longitudinal variation of the maximum axial stress $\bar{\sigma}_x$ in the elastic substrate $(-0.5h)$ and piezoelectric layer $(+0.6h)$ of the beam $(S = 10)$ under load case 1: Comparison with continuum-based FE solution.

### 3.2 Free Vibration Analysis

In this section, we perform the free vibration analysis of the same composite beam (shown in Fig. 1) with PZT-patch of length $a_p = 0.15a$ and thickness $h_p = 0.5h$ to assess the proposed SE model in comparison with the continuum-based FE solution. This piezoelectric-patched beam is fixed at $x = 0$ and pinned at $x = l$. We also compare the free vibration response using the present method with and without the continuity model for satisfying the continuity at the patch fronts.

We determine the natural frequencies ($f_n = w_n/2\pi$) for the first three modes, for which the present ZIGT-based SE with HPLSC model yielded the converged solution with only 2 and 3 eight-node elements for hybrid and elastic part, respectively. We keep the same mesh in the elastic substrate for continuum-based FE solution a sin the static analysis but employed $15 \times 6$ (length $\times$ thickness) CPS8R elements in the piezoelectric patch layer. Table 3 presents these results for beam $S = 10$ and 20 using the present method with and without continuity model with a similar number of DOFs. They are compared with the continuum-based 2D FE solution. It shows that the results employing the continuity model are in good agreement, whereas the solution without satisfying the continuity at the patch front gives a significant error. Thus, it shows the importance of satisfying the continuity at the patch front due to the difference in the

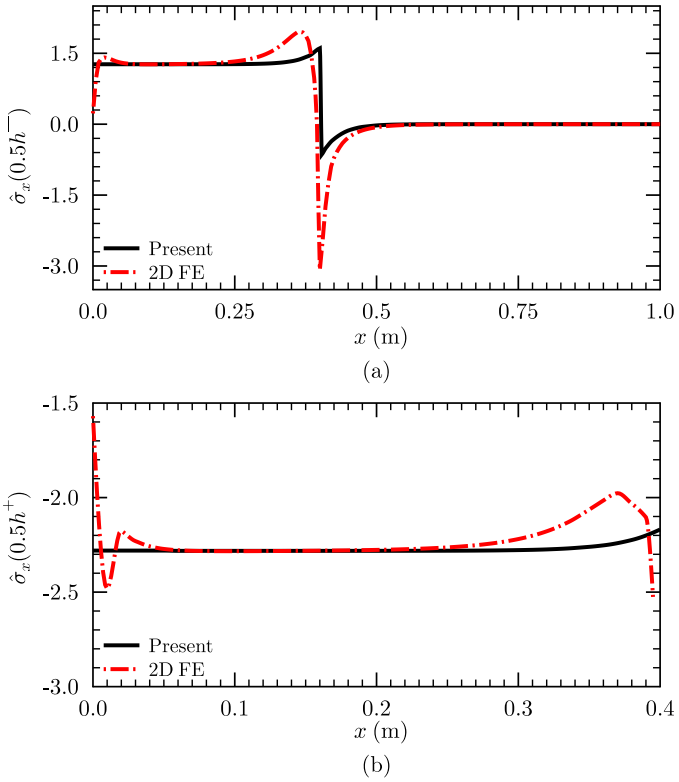


**Figure 5**: Longitudinal variation of the maximum axial stress $\hat{\sigma}_x$ in the elastic substrate ($0.5h^-$) and piezoelectric layer ($0.5h^+$) of the beam ($S = 10$) under load case 2: Comparison with continuum-based FE solution.

in-plane displacement variation in the hybrid and elastic parts.

**Table 3**: Natural frequencies (Hz) of first three modes of a fixed-pinned composite beam ([0°/90°]) with piezoelectric patch at the top of the elastic substrate: Comparison of the present method with and without employing continuity model with the continuum-based solution.

| | | Present | Present | | % error (Present) | |
|---|---|---|---|---|---|---|
| | Mode | (with continuity) | (w/o continuity) | 2D FE | with continuity | w/o continuity |
| $S = 10$ | 1 | 546.85 | 510.57 | 534.29 | 2.35 | -4.44 |
| | 2 | 1269.02 | 1293.10 | 1244.03 | 2.01 | 3.94 |
| | 3 | 1976.33 | 2073.19 | 1871.20 | 5.62 | 10.79 |
| $S = 20$ | 1 | 348.34 | 329.96 | 344.82 | 1.02 | -4.31 |
| | 2 | 919.81 | 920.62 | 913.74 | 0.67 | 0.75 |
| | 3 | 1529.65 | 1564.94 | 1494.59 | 2.35 | 4.71 |

## 4 CONCLUSIONS

A time-domain spectral element has been developed based on the efficient electromechanically coupled layerwise ZIGT for analysis of laminated composite beams integrated with patch piezoelectric actuators and sensors. The ZIGT enjoys the advantages of the high accuracy of the LWTs and the high computational efficiency of the ESL theories. The formulation incorporates the HPLSC method for satisfying the continuity of the displacement field at the patch fronts. A detailed numerical study has been investigated to evaluate the performance of the proposed element for static and free vibration analyses of smart composite beams equipped with piezoelectric patches under mechanical and electrical potential loadings, from which the following conclusions can be drawn.

- The proposed SE in conjunction with the HPLSC model gives excellent results for the deflection and stresses in moderately thick to thin beams under mechanical and electrical loadings in comparison with the continuum-based FE solution.

- The present model yields good results also for natural frequencies of moderately thick to thin smart composite beams. In contrast, the present method without a continuity model at the patch front gives inaccurate results, showing the importance of continuity criteria for modelling the patch transducers.

The current formulation will be extended for assessing the delamination using wave propagation analysis in the laminated structures with the help of bonded piezoelectric actuators and sensors, which will benefit the model-based SHM and physics-assisted data-driven SHM of such smart structures featuring delamination damage.

## REFERENCES

[1] V. Giurgiutiu, B. Lin, G. Santoni-Bottai, and A. Cuc, "Space application of piezoelectric wafer active sensors for structural health monitoring," *Journal of Intelligent Material Systems and Structures*, vol. 22, no. 12, pp. 1359–1370, 2011.

[2] E. F. Crawley and J. De Luis, "Use of piezoelectric actuators as elements of intelligent structures," *AIAA journal*, vol. 25, no. 10, pp. 1373–1385, 1987.

[3] G. Shankar, P. K. Mahato, and S. Keshava Kumar, "Transient analysis and control of delaminated composite plates in hygrothermal environment using active fiber composite actuator," *Mechanics of Advanced Materials and Structures*, vol. 27, no. 16, pp. 1412–1432, 2020.

[4] C. E. Seeley and A. Chattopadhyay, "Modeling of adaptive composites including debonding," *International Journal of Solids and Structures*, vol. 36, no. 12, pp. 1823–1843, 1999.

[5] S. Kapuria and A. Ahmed, "A coupled efficient layerwise finite element model for free vibration analysis of smart piezo-bonded laminated shells featuring delaminations and

transducer debonding," *International Journal of Mechanical Sciences*, vol. 194, p. 106195, 2021.

[6] R. Lee and A. C. Cangellaris, "A study of discretization error in the finite element approximation of wave solutions," *IEEE Transactions on Antenna and Propagation*, vol. 40, no. 5, pp. 542–549, 1992.

[7] D. Siorikis, C. Rekatsinas, N. Chrysochoidis, and D. Saravanos, "An extended layerwise spectral finite element framework for delamination growth simulation in laminated composite strips," *Composite Structures*, vol. 276, p. 114452, 2021.

[8] S. Kapuria and M. Jain, "A $C^1$-continuous time domain spectral finite element for wave propagation analysis of Euler–Bernoulli beams," *International Journal for Numerical Methods in Engineering*, vol. 122, no. 11, pp. 2631–2652, 2021.

[9] M. Jain and S. Kapuria, "Time-domain spectral finite element based on third-order theory for efficient modelling of guided wave propagation in beams and panels," *Acta Mechanica*, vol. 233, no. 3, pp. 1187–1212, 2022.

[10] M. Jain and S. Kapuria, "$C^1$-continuous time-domain spectral finite element for modeling guided wave propagation in laminated composite strips based on third-order theory," *Composite Structures*, vol. 289, p. 115442, 2022.

[11] M. Jain, S. Kapuria, and S. Pradyumna, "Efficient time-domain spectral element with zigzag kinematics for multilayered strips," *International Journal of Mechanical Sciences*, vol. 232, p. 107603, 2022.

[12] A. Ahmed and S. Kapuria, "Third order theory based quadrilateral element for delaminated composite plates with a hybrid method for satisfying continuity at delamination fronts," *Composite Structures*, vol. 181, pp. 84–95, 2017.

[13] C. Ramadas, K. Balasubramaniam, M. Joshi, and C. Krishnamurthy, "Interaction of guided Lamb waves with an asymmetrically located delamination in a laminated composite plate," *Smart Materials and Structures*, vol. 19, no. 6, p. 065009, 2010.